ACS APPLIED MATERIALS & INTERFACES

RESEARCH ARTICLE

www.acsami.org

C_{60} Fullerene Nanocolumns–Polythiophene Heterojunctions for Inverted Organic Photovoltaic Cells

Michael Thomas,[†,‡] Brian J. Worfolk,[‡,§] David A. Rider,[#,‡,§] Michael T. Taschuk,[†,‡] Jillian M. Buriak,[‡,§] and Michael J. Brett[*,†,‡]

[†]Department of Electrical and Computer Engineering, University of Alberta, Edmonton, Alberta T6G 2V4, Canada

[‡]NRC National Institute for Nanotechnology, Edmonton, Alberta T6G 2M9, Canada

[§]Department of Chemistry, University of Alberta, Edmonton, Alberta T6G 2G2, Canada

Supporting Information

ABSTRACT: Inverted organic photovoltaic cells have been fabricated based on vertical C_{60} nanocolumns filled with spin-coated poly[3-(4-carboxybutyl)thiophene-2,5-diyl] (P3CBT). These C_{60} nanocolumns were prepared via glancing angle deposition (GLAD), an efficient synthetic approach that controls the morphology of the resulting film, including intercolumn spacing, nanostructure shapes, and overall film thickness, among others. Intercolumn spacing was tuned to better match the expected P3CBT exciton diffusion length while simultaneously increasing heterointerface area. Due to observed in situ dissolution of the C_{60} nanocolumns in solvents typically used to spin-coat polythiophene-based polymers (i.e., chloroform and chlorobenzene), the carboxylic acid-substituted polythiophene, P3CBT, was used as it is soluble in dimethyl sulfoxide (DMSO), a solvent that did not affect the structure of the GLAD-produced C_{60} nanostructures. Preservation of the C_{60} nanocolumnar structure in the presence of DMSO, with and without P3CBT, was verified by absorbance spectroscopy and SEM imaging. Incorporating these nanostructured C_{60}/P3CBT films into photovoltaic devices on indium tin oxide (ITO) showed that the engineered nanomorphology yielded a 5-fold increase in short-circuit current and a power conversion efficiency (PCE) increase from (0.2 ± 0.03)% to (0.8 ± 0.2)% when compared to a planar device. When compared to a standard bulk heterojunction (BHJ) device based upon the same materials, the C_{60}-GLAD device outperformed fully solution-processed bulk heterojunctions, which were observed to have PCEs of (0.49 ± 0.03) %.

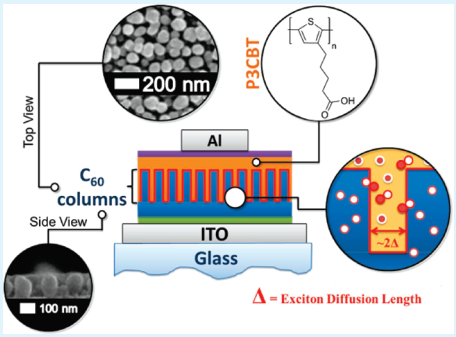

KEYWORDS: organic photovoltaics, nanocolumns, bulk heterojunction, glancing angle deposition, inverted photovoltaics, solar cells, C_{60} fullerene, poly[3-(4-carboxybutyl)thiophene]

1. INTRODUCTION

Organic photovoltaic (OPV) devices are promising candidates for low-cost solar cells.[1−13] While significant progress has been made in optimizing this class of solar cells, the short exciton diffusion lengths limit the thickness of the photoactive layer and consequently restrict light absorption.[14] The development of bulk heterojunctions (BHJs) increased the heterointerfacial area and reduced feature sizes to approach that of exciton diffusion lengths, which has allowed for casting thicker photoactive films.[15] A widely researched BHJ is assembled from a two-component photoactive layer of the electron-donating, regioregular 2,5-diyl-poly(3-hexylthiophene) (P3HT) polymer and the electron-accepting [6,6]-phenyl-C_{61}-butyric acid methyl ester (PCBM) fullerene.[9,16−19] Typical BHJs exhibit a disordered morphology in the photoactive layer, resulting in pocket domains and dead ends, and thereby limit charge carrier transport.[20] Therefore, achieving ordered morphologies by manipulating the network of donor and acceptor molecules on the nanoscale[21] or using self-assembly techniques[22,23] can greatly improve device performance.

An architecture based on an interpenetrating network of vertical nanocolumnar donor and acceptor materials is postulated to maximize charge transport and minimize dead-ends.[6,24] We have previously developed a nanocolumn fabrication method known as glancing angle deposition (GLAD) which utilizes physical vapor deposition at oblique angles.[25] GLAD films are deposited from a highly collimated flux source onto a substrate that can be tilted and rotated. Ballistic shadowing of the molecular flux enables fabrication of porous nanoscale architectures such as slanted and vertical columns, helices, and chevrons.[26]

In terms of prior PV devices based upon GLAD, this synthetic approach has been used to fabricate vertical or slanted nanocolumns for indium tin oxide electrodes,[27] dye-sensitized solar cells with titanium dioxide,[28] for hybrid TiO_2/polythiophene devices,[29] and for OPV with small molecule donor materials such as copper phthalocyanine (CuPc).[30−32] Although previous work has demonstrated GLAD C_{60} columns on silicon and indium tin

Received: January 20, 2011
Accepted: April 27, 2011
Published: April 27, 2011

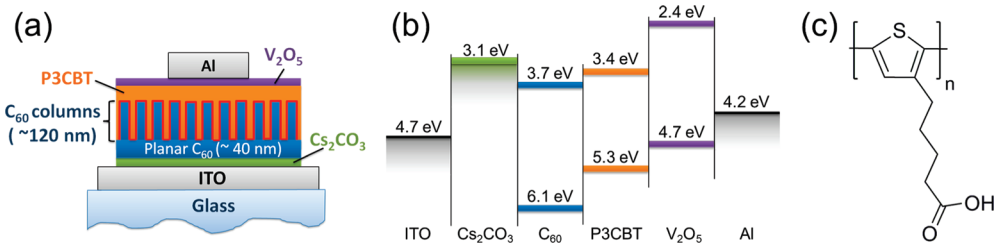

Figure 1. (a) Architecture for an inverted OPV device based on nanostructured C_{60}/P3CBT multilayers. (b) Corresponding electronic structure for the proposed device architecture. (c) P3CBT monomer.

oxide (ITO) coated substrates,[33] here we fabricate a complete inverted solar cell incorporating GLAD C_{60} nanocolumns (Figure 1 a,b). We subsequently investigate the stability of the C_{60} nanostructures to solvents in an effort to develop a procedure for introducing a complementary donor polymer phase to complete the photoactive layer. It was found that solvents for conventional donor polymers like poly(3-hexylthiophene) (P3HT) dissolve C_{60} films, including an array of aromatic and halogenated solvents. Accordingly, a spin-coating process based on dimethyl sulfoxide (DMSO)-soluble poly[3-(4-carboxybutyl)thiophene-2,5-diyl] (P3CBT)[34] (Figure 1 c), which preserves film morphology is reported. P3CBT has similar optoelectronic properties as P3HT with respect to energy levels, absorption spectra and photoluminescence. Through the effective nanostructure control possible with GLAD, column spacing can be adjusted to better match the donor polymer exciton diffusion length and simultaneously increase P3CBT/C_{60} interface area. Using this approach, GLAD structured OPVs with a power conversion efficiency (PCE) of (0.8 ± 0.2) % were produced, outperforming a planar double layer device with (0.2 ± 0.03) % PCE, as well as a BHJ with (0.49 ± 0.03)% PCE.

2. EXPERIMENTAL SECTION

Film Deposition. C_{60} powder (Sigma Aldrich, SES Research, 99.9% pure) was deposited on ITO coated glass substrates (thickness ~130 nm, sheet resistance ~20 Ω sq^{-1}). Before evaporation, the C_{60} powder was purified at 250 °C for 12 h in the deposition chamber at a pressure of 1×10^{-7} Torr. Thermal evaporation was performed from an alumina crucible (Delta Glass) at an evaporation temperature of 450 °C and a working pressure of 2×10^{-7} Torr. Deposition rates between 0.5 Å s^{-1} to 1 Å s^{-1} were achieved and measured with a quartz crystal thickness monitor. Film morphology was controlled by depositing at different substrate angles α = 75, 80, and 85°. Rotation speeds ranged from 0.2 to 0.6 rpm to maintain a constant pitch of 24 nm, i.e., a full substrate turn per 24 nm of film growth.

Device Fabrication and Testing. ITO coated glass substrates were sequentially sonicated in methylene chloride, Millipore water (18 MΩ.cm) and 2-propanol for 10 min each. A 10 min air plasma was then performed with a Harrick plasma (PDC 32G, 18 W) cleaner at ~0.1 Torr. Cs_2CO_3 was used as a cathodic interfacial modifier and was cast from a 0.2 wt % solution in 2-ethoxyethanol forming a ~1 nm thick layer. The substrate was then annealed at 150 °C for 20 min as previously reported.[35] The substrates were then pumped into the GLAD vacuum chamber for deposition of C_{60} films. Substrates were removed from the chamber under Ar flow and transferred to a desiccator purged with Ar to limit the air exposure of the C_{60} films and oxidation of the surface. C_{60} films were immediately (~10 min) transferred to a nitrogen filled glovebox. P3HT and P3CBT (30 mg mL^{-1}) in *o*-dichlorobenzene and dimethyl sulfoxide (DMSO) respectively were filtered with a 0.2 μm PTFE filter and spun-on directly onto the C_{60} films at 600 rpm for 10 min. Films were then annealed at 50 °C for 20 min. V_2O_5 (20 nm) and Al (70−80 nm) were deposited by thermal evaporation at a rate of 0.01 and 5 Å s^{-1}, respectively. Devices are fabricated in sets of 5 per substrate, with a (0.155 ± 0.008) cm^2 device area. For each deposition angle, multiple devices were fabricated and characterized. For power conversion efficiency the maximum achieved value is given, as well as an average of at least 10 devices prepared which are arranged in parallel on at least 2 different ITO chips originating from one process. *J*−*V* curves were measured using an Oriel 91191 1000 W solar simulator with a Keithley 2400 source meter. Light intensity was adjusted using a calibrated Si solar cell (NREL certified) with a KG-5 filter (PV Measurements, Inc., model PVM624).

Analysis of Morphology. The resulting nanostructures were analyzed using a Hitachi S-4800 secondary electron microscope (SEM) and a JEOL JSM-6301 FXV SEM. Film thicknesses range from 80 to 120 nm and are measured with the SEM at an estimated uncertainty of 10%. This error has been added in quadrature to precision error throughout the paper. SEM images were analyzed using ImageJ 1.42q.[36] Average column spacings and diameters were measured statistically from top view SEM images.

Crystal Structure. The crystal structure of the films deposited on ITO/glass was investigated using Bragg−Brentano X-ray diffractometry (XRD) with a Bruker D8 Discover with GADDS using Cu−K_α (λ = 1.541 Å) radiation. Since films were thin, the XRD was performed at a grazing incidence angle of ω = 2°. For measuring full-width-at-half-maximum, average instrumental aperture of 0.31° was accounted for as a systematic error.

Optical Measurements. Absorbance measurements of C_{60}-only, C_{60}/P3HT and C_{60}/P3CBT multilayer films were performed with a spectrophotometer (Perkin-Elmer NIR-UV Lambda 900). Planar C_{60} films (~170 nm) and nanostructured C_{60} films (~50 nm planar + ~120 nm GLAD) on fused silica substrates were used as the base layer. P3HT and P3CBT were added by the spin coating process described above. The multilayers were dried on a hot plate at 50 °C for 20 min in a nitrogen atmosphere.

Photoluminescence of P3CBT-only, GLAD C_{60}-only and C_{60}/P3CBT multilayer films on quartz substrates was measured using a 442 nm He−Cd laser as the excitation source. Scattered 442 nm light was filtered with a long pass filter (475 nm, TR Laboratories). The remaining photoluminescence was measured with a compact CCD spectrometer (Ocean Optics USB2000, 300 nm -1050 nm). The spectral responsivity of the compact CCD spectrometer was corrected using a blackbody source (HL-2000-FHSA-LL). Integration time was 500 ms for all measurements, and a dark spectrum was subtracted in each case. To account for film thickness differences, we normalized the P3CBT-only absorbance spectrum to the thickness of the P3CBT in the multilayered samples.

Microtome Transmission Electron Microscopy. Multilayer films were embedded in spurs epoxy resin and cured at 70 °C for 8 h. The product was dipped sequentially in liquid nitrogen and water to crack the film from the glass. The resulting supported film was microtomed with a diamond blade. The cross sections were floated onto carbon coated

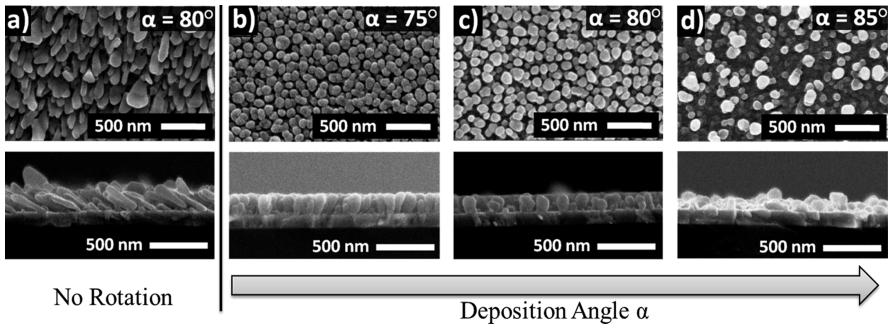

Figure 2. (a) Top and side views of a C_{60} film deposited by GLAD at α = 80° with no substrate rotation. The growth results in slanted columns tilted by $\beta = 60° \pm 5°$ from the normal vector of the substrate. (b–d) Vertical columnar C_{60} GLAD films deposited with continuous rotation at α = 75, 80, and 85°, respectively.

Table 1. Summary of Column Diameters and Intercolumn Spacing of C_{60} Films Grown at Different Deposition Angles α

morphology	deposition angle α (deg)	column diameter (nm)	column spacing (nm)
tilted columns	80	60 ± 10	50 ± 10
vertical columns	75	90 ± 10	40 ± 20
vertical columns	80	90 ± 10	65 ± 20
vertical columns	85	100 ± 20	180 ± 90

transmission electron microscope (TEM) grids and viewed with a JEOL JEM 2100 TEM with an accelerating voltage of 120 kV.

3. RESULTS AND DISCUSSION

3.1. Control of Column Morphology and Spacing. To investigate the scope of C_{60} film morphology obtainable via GLAD, tilted and vertical C_{60} nanocolumns were fabricated on ITO-coated glass at deposition angles (α) of 75, 80, and 85°, with and without sample rotation. Figure 2 shows SEM images with top and side views of the nanostructured films. Films deposited at an angle α of 80° (Figure 2a) have a thickness of 210 nm ±30 nm and an average column tilt angle (β, measured from substrate normal) of 60° ± 5°. This value agrees with the prediction from Tait's ballistic model[37] of $\beta = 56°$. The average midheight column diameter is 60 nm ±10 nm and the average column length is 350 nm ±50 nm. During the GLAD deposition process, substrate rotation concurrent with deposition creates an isotropic distribution of flux over initial nuclei that form on the surface, resulting in vertically oriented columns. The SEM images of C_{60} films, shown in Figure 2b–d, show vertical C_{60} nanocolumns that were deposited with rotation, at angles of 75, 80, and 85°. Average column diameter and intercolumn spacing are given in Table 1. For C_{60} vertical posts deposited between 75 and 85°, column diameter does not depend strongly on deposition angle, however the average intercolumn spacing is 40 nm ± 20 nm and 65 nm ±20 nm for films deposited at angles of 75 and 80°, respectively. Intercolumn spacing increases nonlinearly, however, to 180 nm ± 90 nm at a deposition angle of 85°, in agreement with ballistic simulations.[37]

At higher deposition angles (α = 85°) of C_{60}, GLAD post heights become less uniform, increasing the relative thickness of the nanocolumn/air interface, an effect previously observed for inorganic GLAD films.[38−40] As is well-known for GLAD films, the C_{60} film density is inversely proportional to deposition angle, with higher densities at lower deposition angles of α, following Tait's ballistic approximation for normalized film density.[26] Optical absorbance measurements reveal the effect of varying film density (see Figure 3). As deposition angle α increases, the density of deposited material and corresponding absorbance decreases. As this ensemble of results shows, through control of substrate orientation during deposition, the GLAD technique enables the deposition of C_{60} nanocolumns with tunable structures.

In excitonic photovoltaic cells, the exciton diffusion length can be a limiting factor, as stated earlier.[14,41] One optimization route for a given organic PV material system is to increase surface area while reducing exciton diffusion paths. For GLAD, this route corresponds to increasing film thickness while matching intercolumn spacing to the exciton diffusion length, by controlling the deposition angle. The carboxylic acid-functionalized polythiophene polymer, P3CBT (Figure 1 c), has an expected exciton diffusion length of 5–20 nm.[6,10,13,42] Of the deposition angles studied here, 75° provides the architecture best matched to the diffusion length. While in principle it would be possible to further reduce intercolumn spacing, this demand must be balanced by the ease of infiltration of the P3CBT into the GLAD nanostructure; these characteristics are discussed below.

3.2. Crystallinity of the C_{60} Nanocolumn Films. Previous studies of planar C_{60}[43,44] and nanostructured C_{60} columnar[33] films have shown them to be polycrystalline . Figure 4 shows XRD results for the GLAD-deposited C_{60} films deposited on ITO electrodes. All three films exhibit a polycrystalline structure with crystallites predominantly oriented in {111} and {220} planes. The *d*-spacings of the films are observed at 8 Å and 5 Å for the {111} and {220} planes, respectively. Other C_{60} peaks have not been observed. These values are in agreement with previously reported C_{60} polycrystalline films and, together with the Miller indices selection rules, indicate a face-centered cubic structure with a resulting lattice constant of 14 Å. Crystallite sizes were determined using the Scherrer equation for spherical crystallites and are given in Table 2.[45] The crystallites appear to be somewhat larger in the nanostructured GLAD C_{60} films as compared to the planar films (α = 0°).

In the planar C_{60} film, both the {111} and {220} planes have comparable intensities, but it can be noted that the {111} plane has a slightly higher intensity in the planar film, whereas in the columnar film, the {220} orientation is stronger. These results suggest that during GLAD deposition, {220} oriented crystallites are more favorably grown than {111} oriented crystal planes. Similar preferential growth has been previously observed in nanocolumns formed by GLAD.[46]

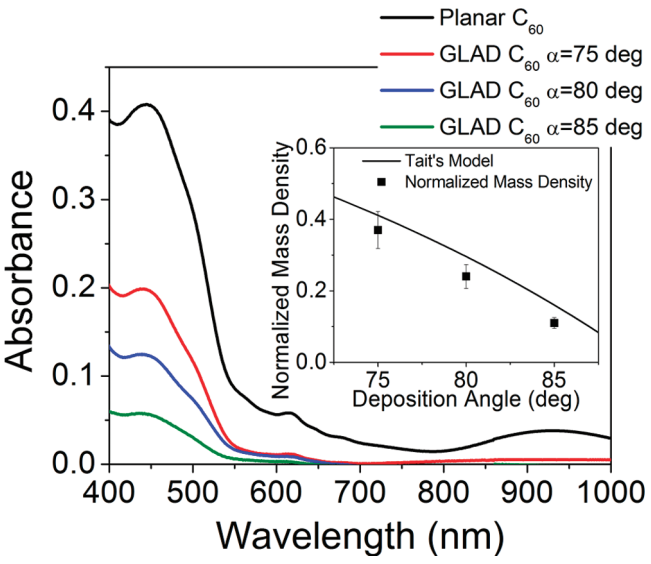

Figure 3. Absorbance measurements of C_{60} films prepared by GLAD at different deposition angles (α). Spectra are normalized to film thickness. The inset shows the normalized mass density as derived from the given absorbance measurements. The dashed curve shows Tait's approximation for the normalized film density (normalized to a film deposited at normal incidence angle).

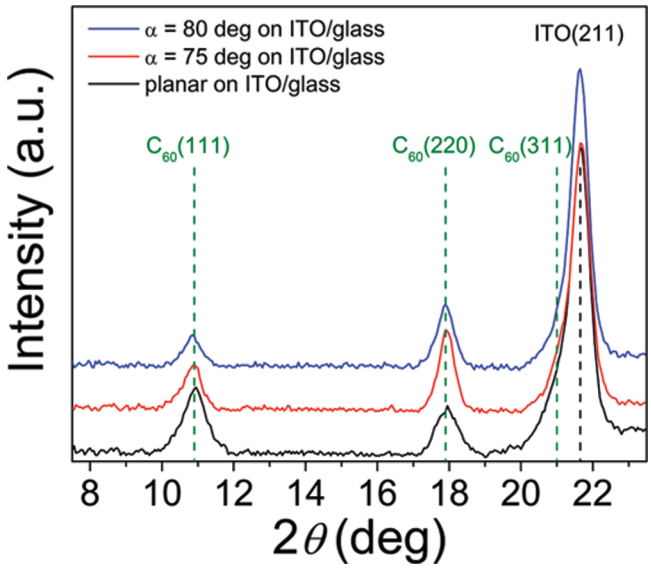

Figure 4. X-ray diffraction measurement of a planar and nanostructured C_{60} film on an ITO/glass substrate with linear intensity. The top two measurements (vertical order in legend follows vertical sequence of measurements) show the diffraction pattern for a film deposited at α = 80° and α = 75°, respectively. The bottom measurement (black) represents the planar C_{60} film. Dotted vertical lines mark the peak positions for the crystallographic orientations in each material.

Table 2. Comparison of Crystallite Sizes of C_{60} Films for the {111} and {220} Phase in the Planar and Nanostructured Films

	crystallite size (nm)	
deposition angle (deg)	{111} phase	{220} phase
0	20	22
75	30	43
80	33	34

3.3. Incorporation of the C_{60} Films into Bulk Heterojunctions. Inverted architecture bulk heterojunction organic photovoltaics have been previously demonstrated, with power conversion efficiencies approaching 4.5%.[35,47−52] In this work, we endeavored to fabricate inverted polymer-fullerene heterojunctions, utilizing the C_{60} films prepared by GLAD as the platform on which these devices were built. Both the planar and GLAD C_{60} films prepared in this study were soluble in common solvents normally used to solubilize the "standard" BHJ polymer, P3HT, including chloroform, dichlorobenzene, chlorobenzene, and dichloromethane. Immersion of the GLAD C_{60} films in all of these solvents resulted in their destruction and dissolution. A rigorous study investigating numerous solvents was conducted and it was found that the C_{60} films were very stable in dimethyl sulphoxide (DMSO) and acetonitrile. As evidence of C_{60} stability in DMSO, both optical absorbance and morphology evaluation was performed before and after rinsing a film in DMSO for 60 s. Negligible change in film absorbance was observed, and SEM measurements confirmed that the nanostructuring is maintained (see the Supporting Information).

Members of the P3CBT family of polymers (Figure 1c) have been previously reported to be soluble in DMSO, and thus this group of polymers seemed to have properties complementary to the GLAD-prepared C_{60} nanocolumns. P3CBT has similar optoelectronic properties as P3HT,[53,54] and previously published P3CBT:PCBM bulk heterojunctions were shown to have power conversion efficiencies of 0.9%.[55] From X-ray diffraction measurements we found that the P3CBT forms crystallites of size about 5 nm, distributed within a matrix of significantly larger PCBM clusters.[55] This can be attributed to the lower solubility of PCBM in the solvents. This is the first report of inverted-mode P3CBT:PCBM OPVs which are fabricated under the same conditions as the forward-mode cells but with different interfacial modifiers. As a result of these characteristics, we proceeded to synthesize nanostructured C_{60} column/P3CBT polymer heterojunctions via spin-coating of the polymer from DMSO, onto the GLAD films. Cross-sectional SEM images show what is apparently good infiltration of the donor polymer into the C_{60} nanostructure fabricated at α = 75° (see Figure 5a), but closer analysis of a microtomed sample by TEM (Figure 5b) shows voids between the C_{60} nanocolumns where polymer does not fully make contact with the C_{60}. This result may be due to a high viscosity of the DMSO,[56] but it is clear that the interfacial area between the C_{60} and polymer is still higher than of a planar interface.

3.4. Light Absorption and Exciton Quenching in C_{60}/P3CBT Heterojunctions. Absorbance spectra of GLAD C_{60}/P3CBT films are shown in Figure 6. The multilayer structures are comprised of the following layers: fused silica/planar C_{60} (∼50 nm)/GLAD C_{60} (∼120 nm)/P3CBT for the GLAD structures, and fused silica/C_{60}(∼170 nm)/P3CBT for the planar film. C_{60} absorption peaks are observed at 266 and 346 nm, and the broad feature at ∼550 nm is due to the C_{60} peak at 455 nm (compare with Figure 3) convolved with another from the P3CBT. As the processing for the P3CBT layer was identical for all films (spin coating), and the fact that this overlapping C_{60}/P3CBT feature varies with deposition angle, it is apparent the absorption results primarily from the C_{60} constituent of the

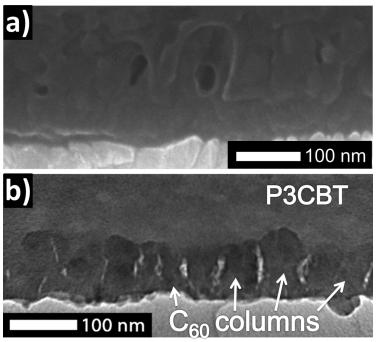

Figure 5. Cross-sectional electron microscopy images of C_{60} nanostructures, fabricated at $\alpha = 75°$, with spun-on P3CBT. (a) SEM image (secondary-electron mode) image. To increase the contrast of the C_{60} columns, the measurement stage was tilted by 10° toward the detector. (b) TEM image (bright-field).

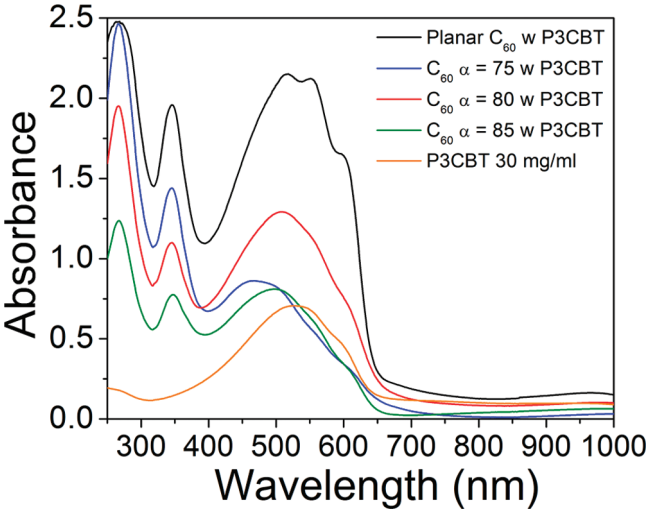

Figure 6. Absorbance spectra of nanostructured C_{60} films with spun-on P3CBT (30 mg mL^{-1}), as well as the spectrum for a single P3CBT layer (orange curve).

heterojunction. The P3CBT peak onset appears at 650 nm, indicating an optical band gap of 1.9 eV. The P3CBT peak at 553 nm is caused by the $\pi-\pi$ stacking of thiophene rings, which leads to increased absorption in the bulk polymer, and increases with a higher degree of ordering.[55]

To estimate exciton quenching for different morphologies, photoluminescence (PL) spectra of GLAD-based C_{60}/P3CBT heterojunctions on silica were taken and compared with planar films. These samples were fabricated simultaneously with the OPV devices described below and thus should have comparable architectures. In addition, a single P3CBT film, and planar C_{60} film were fabricated on silica as references. As can be seen in Figure 7, significantly more excitons were quenched in the GLAD C_{60}/P3CBT film as compared to the planar films. Interestingly, the exciton quenching for the multilayer made at $\alpha = 75°$ was slightly less than for $\alpha = 80°$, although the $\alpha = 75°$ device performed better (vide infra). The J_{SC} might be larger for $\alpha = 75°$ because of a higher mass density of the polycrystalline C_{60} film providing an enhanced conductive path, but the reasons for this behavior are not yet fully understood.

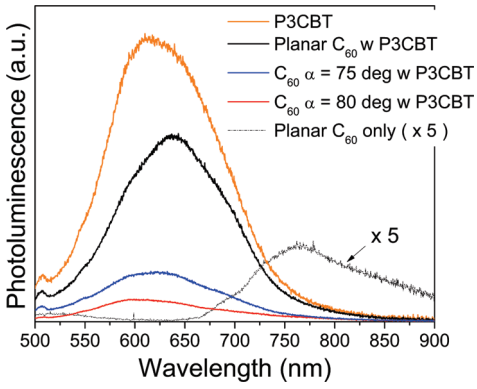

Figure 7. Photoluminescence spectra of samples on silica substrates. A single P3CBT film is shown together with C_{60}/P3CBT double layers, as well as the magnified spectrum of a planar C_{60} GLAD film.

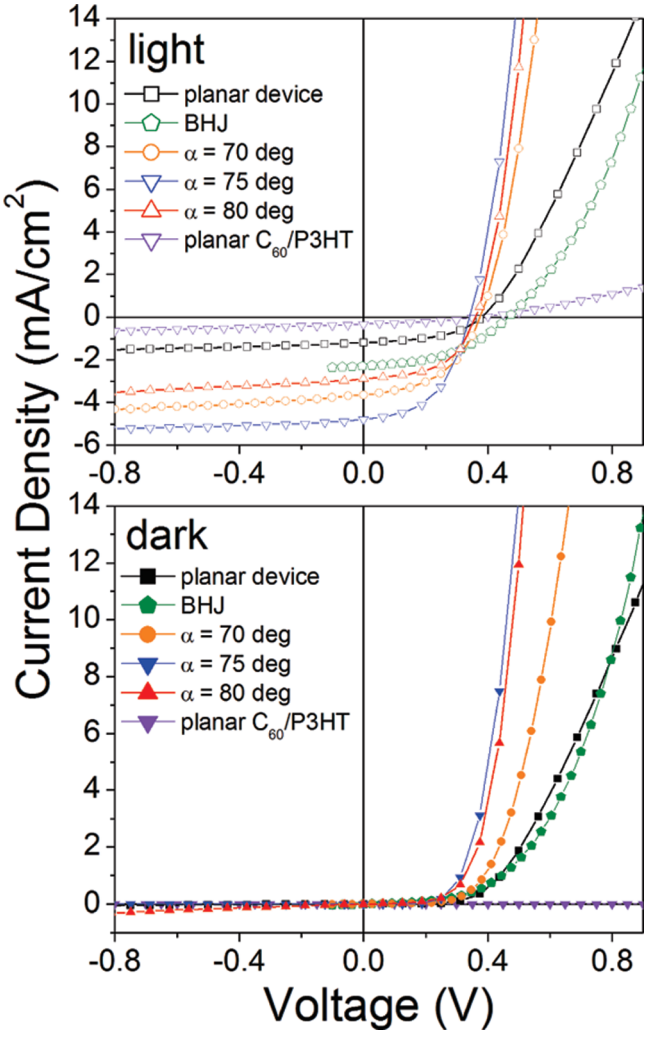

Figure 8. $J-V$ characteristics of OPVs. Devices based on planar C_{60} (glass/ITO/Cs_2CO_3/C_{60}(planar)/P3CBT/V_2O_5/Al) and C_{60} GLAD films fabricated at $\alpha = 80°$, $\alpha = 75°$, and $\alpha = 70°$ (glass/ITO/Cs_2CO_3/C_{60}(planar)/$C_{60}(\alpha)$/P3BCT/V_2O_5/Al) are shown. For comparison, a BHJ (glass/ITO/Cs_2CO_3/P3CBT:PCBM/V_2O_5/Al)[55] and a planar C_{60} device with P3HT as donor polymer are included.

Table 3. Comparison of Inverted OPV Based on Planar and Nanostructured C_{60} Films. All Devices Have the Following Architecture: Glass/ITO/Cs_2CO_3/ Active Layer/V_2O_5/Al[a]

active layer	J_{SC} (mA/cm^2)	V_{OC} (V)	FF	PCE (%)	best PCE (%)
C_{60} planar/P3CBT	0.92 ± 0.05	0.37 ± 0.01	0.55 ± 0.05	0.20 ± 0.03	0.23
C_{60} planar/C_{60}(α = 70°)/P3CBT	3.20 ± 0.25	0.34 ± 0.02	0.42 ± 0.04	0.47 ± 0.08	0.66
C_{60} planar/C_{60}(α = 75°)/P3CBT	4.60 ± 0.20	0.33 ± 0.01	0.45 ± 0.01	0.80 ± 0.20	1.00
C_{60} planar/C_{60}(α = 80°)/P3CBT	3.02 ± 0.12	0.35 ± 0.02	0.47 ± 0.06	0.56 ± 0.06	0.62
P3CBT: PCBM	2.25 ± 0.05	0.45 ± 0.02	0.44 ± 0.01	0.49 ± 0.03	0.52
C_{60} planar/P3HT	0.30 ± 0.10	0.30 ± 0.17	0.33 ± 0.14	0.03 ± 0.03	0.05

[a] For comparison, a BHJ based on P3CBT is added.[55] In addition, data for a GLAD C_{60} device with P3HT is shown. Variance is higher for P3HT since the process does not provide consistent results because of the dissolution of the C_{60} layer. (For all data presented here, at least 2 ITO chips with a minimum of 10 devices were tested.).

3.5. Inverted OPV Devices Based on C_{60}/P3CBT Heterojunctions. To match the exciton diffusion length of polythiophenes, about 5 to 20 nm, the C_{60} column spacing should be between 10 to 40 nm. OPV devices were fabricated starting with nanostructured C_{60} films produced at α = 75° and 80°, resulting in an average column spacing of about 40 and 65 nm, respectively. The overall electronic structure of the device is shown in Figure 1 b. To improve charge selection and extraction, a layer of Cs_2CO_3 (~1 nm) was incorporated as an electron transport layer, and V_2O_5 (~10 nm) as the hole transport layer, on their respective electrodes. These transport layer materials have been found to increase power conversion efficiency in inverted devices.[57−60] $J-V$ characteristics of fabricated devices are shown in Figure 8. Comparing light curves, OPVs based on the C_{60}/P3CBT heterointerface have similar open-circuit voltages (V_{OC}), but the short-circuit current density (J_{SC}) depends on C_{60} film morphology. The device made at α = 75° exhibits the highest short-circuit current at 4.60 ± 0.20 mA/cm^2. As a comparison, the characteristic curve of a BHJ based on P3CBT:PCBM is shown - while the J_{SC} is lower than in both GLAD C_{60} cells, the V_{OC} is slightly higher. Although P3CBT has similar optoelectronic properties as P3HT, the hole mobility has been reported to be 1.5×10^{-4} cm^2 V^{-1} s^{-1}, which is significantly lower than commonly reported values for P3HT (5×10^{-3} cm^2 V^{-1} s^{-1}), which reduces charge transport in the devices.[61]

The dark curves of the GLAD C_{60} cells and the BHJ have comparable slopes above the turn-on voltage, indicating that the series resistance is comparable. Series resistance seems to be higher for the planar C_{60}/P3CBT device than in all previously mentioned OPVs; the interfacial layers and electrodes were fabricated using the same process for these devices, and thus an increase in series resistance can be attributed to less efficient charge extraction from the double layer. To illustrate the dissolution of the C_{60} layer during the spin-coating of P3HT in chloroform, we have added the $J-V$ curve of a planar C_{60}/P3HT device. The very low slope of the dark curve suggests a high resistivity of the architecture, and the corresponding light curve has very low photoactivity. These effects result from dissolution of C_{60} because few C_{60} molecules remain to form a heterointerface with the P3HT.

Table 3 summarizes the results for the prepared devices. The V_{OC} was measured to be (0.37 ± 0.01) V in the planar device which is slightly higher than in all three GLAD devices. Because V_{OC} is highly dependent on device processing,[62] these values indicate a consistent process quality. The V_{OC} in all of our inverted GLAD devices are, however, lower than the value measured in a BHJ based on P3CBT: PCBM (0.45 ± 0.02) V, with the same interfacial layers and electrodes. Although a slight decrease in V_{OC} for the BHJ would be expected due to the different LUMO level in PCBM, which is located at about 4 eV instead of 3.7 eV for the C_{60} films,[63−66] the major difference in V_{OC} is attributed to the atmospheric exposure during the processing of our multilayered devices that might affect the C_{60}/P3CBT interface. In the BHJ device, the OPV is fabricated from a mixed solution including PCBM and P3CBT, and during the spin coating deposition of the BHJ the PCBM:P3CBT interface forms in solution during solvent evaporation, thus reducing the interface's atmospheric exposure. In the GLAD device process, a vacuum break occurs after finishing the C_{60} deposition by GLAD and before the P3CBT spin coating step. Although particular care was used in handling the samples and keeping samples under inert atmosphere during vacuum breaks, some amount of oxygen and moisture contamination of the C_{60} surface is expected,[67] leading to a lower V_{OC} than in the fully solution processed BHJ. In addition, the V_{OC} of the BHJ inverted devices (0.45 V) is lower than previously reported forward-mode BHJ devices (0.60 V)[55] indicating that further tuning of the Cs_2CO_3 and V_2O_5 interfacial modifiers could improve the V_{OC}. With further process improvement and minimization of atmospheric exposure of the C_{60} films, it is expected that V_{OC} and thus PCE can be improved.

With a higher heterointerfacial area and improved matching of the column spacing to the exciton diffusion length, the number of dissociated excitons, and thus J_{SC}, is expected to increase. Table 3 shows a significant increase in J_{SC} for the nanostructured devices relative to the planar samples. The α = 80° and α = 75° GLAD devices show three- and 5-fold respective increases in J_{SC} relative to the planar device. Consequently, the power conversion efficiencies (PCE) for nanostructured devices are significantly higher. Compared with a mean PCE of (0.20 ± 0.03) % in the planar samples, mean PCEs of (0.8 ± 0.2)% and (0.56 ± 0.06)% are achieved in devices fabricated at α = 75° and α = 80°, respectively. Relative to the planar device, the BHJ device showed a 2-fold increase in J_{SC}. This is less than the 5-fold increase of the best GLAD device (α = 75°) and suggests that the ordered interface provided by nanocolumnar C_{60} is an improvement over the disordered BHJ interface, maximizing surface area while maintaining a beneficial morphology for charge transport. A further improvement would be expected when going to lower deposition angles and thus decreasing column spacing to better match the exciton diffusion length of the polymer. The devices fabricated at α = 70° (also see the Supporting Information), however, do not show further improvement. Their J_{SC} is at (3.20 ± 0.25) mA/cm^2 and the achieved PCE is (0.47 ± 0.08) %, which is comparable with the device fabricated at α = 80°. This result is

attributed to poor filling of the polymer into the tightly spaced column array, leading to a decreased photoactive surface area compared with the $\alpha = 75°$ device.

A $J-V$ curve for OPVs can be modeled using diode behavior. Because the quality of a heterointerface in a diode determines the shape of the $J-V$ curve, a change in ideality, i.e., a change in $J-V$ curvature, might occur for different heterointerface configurations. As previously mentioned, P3CBT coverage at the nanostructured C_{60} interface is only partly complete when using DMSO as the solvent (Figure 5b). This may cause $J-V$ curve nonidealities which lower the fill factor (FF) for the nanostructured devices compared with the planar samples.

4. CONCLUSION

Nanocolumn C_{60} films fabricated by glancing angle deposition were filled with P3CBT to fabricate inverted organic photovoltaic cells. A 4-fold increase in PCE demonstrates the importance of interface structuring and morphological control, which allows for improved exciton harvesting. We believe that further improvements in device efficiency may be possible with optimization of polymer filling procedures, reduction of oxygen contamination, and through evaluation of the full morphological space afforded by the nanostructural control of GLAD. The device fabrication process described here affords the potential for low-cost manufacturing, as the GLAD and wet chemical processes may potentially be scaled up for roll-to-roll manufacture. Furthermore, the versatility of the glancing angle deposition process may impact other materials systems where device architectures with nanostructural ordering are beneficial.

■ ASSOCIATED CONTENT

Supporting Information. A solubility study of GLAD structured C_{60} films in dimethyl sulfoxide and chloroform is available, analyzed with absorbance spectroscopy and scanning electron microscopy (SEM). In addition, SEM images of a GLAD C_{60} film deposited at $\alpha = 70°$ are shown. Preliminary postannealing experiments were performed and their effect on device performance was measured. This material is available free of charge via the Internet at http://pubs.acs.org/.

■ AUTHOR INFORMATION

Corresponding Author

*E-mail: mbrett@ualberta.ca.

Present Addresses

#Departments of Chemistry and Engineering Technology, Western Washington University, Bellingham, WA, 98225, USA.

■ ACKNOWLEDGMENT

The authors thank George Braybrook and De-Ann Rollings for SEM imaging, Tate C. Hauger and Dr. Michael D. Fleischauer for device testing, Dr. Ming Chen for assistance with microtome sample preparation, Dr. Jonathan Veinot for access to a glovebox evaporator, Dr. Al Meldrum for access to PL equipment, and Dr. Xuejun Sun of NRC-NINT electron microscopy for assistance with TEM imaging. In addition, we gratefully acknowledge the financial support of the following organizations: Vanier Canada Graduate Scholarships Program, NRC-NINT, NSERC of Canada, the Killam Trusts, Alberta Innovates-Technology Futures (AITF), the School of Energy and the Environment (SEE) at the University of Alberta, the Canada Research Chairs Program, and Micralyne, Inc.

■ REFERENCES

(1) Tang, C. W. *Appl. Phys. Lett.* **1986**, *48*, 183–185.
(2) Sariciftci, N. S.; Smilowitz, L.; Heeger, A. J.; Wudl, F. *Science* **1992**, *258*, 1474–1476.
(3) Halls, J. J. M.; Walsh, C. A.; Greenham, N. C.; Marseglia, E. A.; Friend, R. H.; Moratti, S. C.; Holmes, A. B. *Nature* **1995**, *376*, 498–500.
(4) Shaheen, S. E.; Radspinner, R.; Peyghambarian, N.; Jabbour, G. E. *Appl. Phys. Lett.* **2001**, *79*, 2996–2998.
(5) Xue, J. G.; Uchida, S.; Rand, B. P.; Forrest, S. R. *Appl. Phys. Lett.* **2004**, *84*, 3013–3015.
(6) Coakley, K. M.; McGehee, M. D. *Chem. Mater.* **2004**, *16*, 4533 4542.
(7) Spanggaard, H.; Krebs, F. C. *Sol. Energy Mater. Sol. Cells* **2004**, *83*, 125–146.
(8) Roncali, J. *Chem. Soc. Rev.* **2005**, *34*, 483–495.
(9) Gledhill, S. E.; Scott, B.; Gregg, B. A. *J. Mater. Res.* **2005**, *20*, 3167–3179.
(10) Blom, P. W. M.; Mihailetchi, V. D.; Koster, L. J. A.; Markov, D. E. *Adv. Mater.* **2007**, *19*, 1551–1566.
(11) Lungenschmied, C.; Dennler, G.; Neugebauer, H.; Sariciftci, S. N.; Glatthaar, M.; Meyer, T.; Meyer, A. *Sol. Energy Mater. Sol. Cells* **2007**, *91*, 379–384.
(12) Saunders, B. R.; Turner, M. L. *Adv. Colloid Interface Sci.* **2008**, *138*, 1–23.
(13) Thompson, B. C.; Frechet, J. M. J. *Angew. Chem., Int. Ed.* **2008**, *47*, 58–77.
(14) Gregg, B. A.; Hanna, M. C. *J. Appl. Phys.* **2003**, *93*, 3605–3614.
(15) Yu, G.; Gao, J.; Hummelen, J. C.; Wudl, F.; Heeger, A. J. *Science* **1995**, *270*, 1789–1791.
(16) Li, G.; Shrotriya, V.; Huang, J. S.; Yao, Y.; Moriarty, T.; Emery, K.; Yang, Y. *Nat. Mater.* **2005**, *4*, 864–868.
(17) Reyes-Reyes, M.; Kim, K.; Dewald, J.; Lopez-Sandoval, R.; Avadhanula, A.; Curran, S.; Carroll, D. L. *Org. Lett.* **2005**, *7*, 5749–5752.
(18) Xin, H.; Kim, F. S.; Jenekhe, S. A. *J. Am. Chem. Soc.* **2008**, *130*, 5424–5425.
(19) van Bavel, S. S.; Sourty, E.; de With, G.; Loos, J. *Nano Lett.* **2009**, *9*, 507–513.
(20) Peumans, P.; Uchida, S.; Forrest, S. R. *Nature* **2003**, *425*, 158 162.
(21) Ma, W. L.; Yang, C. Y.; Gong, X.; Lee, K.; Heeger, A. J. *Adv. Funct. Mater.* **2005**, *15*, 1617–1622.
(22) McClure, S. A.; Worfolk, B. J.; Rider, D. A.; Tucker, R. T.; Fordyce, J. A. M.; Fleischauer, M. D.; Harris, K. D.; Brett, M. J.; Buriak, J. M. *ACS Appl. Mater. Interfaces* **2010**, *2*, 219–229.
(23) Briseno, A. L.; Holcombe, T. W.; Boukai, A. I.; Garnett, E. C.; Shelton, S. W.; Frechet, J. J. M.; Yang, P. D. *Nano Lett.* **2010**, *10*, 334–340.
(24) Kim, J. S.; Park, Y.; Lee, D. Y.; Lee, J. H.; Park, J. H.; Kim, J. K.; Cho, K. *Adv. Funct. Mater.* **2010**, *4*, 540–545.
(25) Robbie, K.; Brett, M. J.; Lakhtakia, A. *Nature* **1996**, *384*, 616 616.
(26) Hawkeye, M. M.; Brett, M. J. *J. Vac. Sci. Technol. A* **2007**, *25*, 1317–1335.
(27) Rider, D. A.; Tucker, R. T.; Worfolk, B. J.; Krause, K. M.; Lalany, A.; Brett, M. J.; Buriak, J. M.; Harris, K. D. *Nanotechnology* **2011**, *22*, 085706.
(28) Kiema, G. K.; Colgan, M. J.; Brett, M. J. *Sol. Energy Mater. Sol. Cells* **2005**, *85*, 321–331.
(29) Gerein, N. J.; Fleischauer, M. D.; Brett, M. J. *Sol. Energy Mater. Sol. Cells* **2010**, *94*, 2343–2350.
(30) Van Dijken, J. G.; Fleischauer, M. D.; Brett, M. J., In *Proceedings of the 33rd IEEE Photovoltaic Specialists Conference*; San Diego, CA; IEEE: Piscataway, NJ, 2008; Vol. 1−4, pp 1222−1225.

(31) Zheng, Y.; Bekele, R.; Ouyang, J. M.; Xue, J. G. *Org. Electron* **2009**, *10*, 1621–1625.
(32) Li, N.; Forrest, S. R. *Appl. Phys. Lett.* **2009**, *95*, 123309.
(33) Zhang, J.; Salzmann, I.; Rogaschewski, S.; Rabe, J. P.; Koch, N.; Zhang, F. J.; Xu, Z. *Appl. Phys. Lett.* **2007**, *90*, 193117.
(34) Bäuerle, P.; Gaudl, K.-U.; Wurthner, F.; Sariciftci, N. S.; Neugebauer, H.; Mehring, M.; Zhong, C.; Doblhofer, K. *Adv. Mater.* **1990**, *2*, 490–494.
(35) Liao, H. H.; Chen, L. M.; Xu, Z.; Li, G.; Yang, Y. *Appl. Phys. Lett.* **2008**, *92*, 173303.
(36) Rasband, W. S. *ImageJ*: U.S. National Institutes of Health: Bethesda, MD, 1997−2009.
(37) Tait, R. N.; Smy, T.; Brett, M. J. *Thin Solid Films* **1993**, *226*, 196–201.
(38) Taschuk, M. T.; Hawkeye, M. M.; Brett, M. J. *Handbook of Deposition Technologies for Films and Coatings: Science, Applications and Technology*; William Andrew (Elsevier): Oxford, U.K., 2010.
(39) Frederick, J. R.; D'Arcy-Gall, J.; Gall, D. *Thin Solid Films* **2006**, *494*, 330–335.
(40) Vick, D.; Smy, T.; Brett, M. J. *J. Mater. Res.* **2002**, *17*, 2904 2911.
(41) Gregg, B. A. *J. Phys. Chem. B* **2003**, *107*, 4688–4698.
(42) Gunes, S.; Neugebauer, H.; Sariciftci, N. S. *Chem. Rev.* **2007**, *107*, 1324–1338.
(43) Krakow, W.; Rivera, N. M.; Roy, R. A.; Ruoff, R. S.; Cuomo, J. J. *Appl. Phys. A-Mater.* **1993**, *56*, 185–192.
(44) Krakow, W.; Rivera, N. M.; Roy, R. A.; Ruoff, R. S.; Cuomo, J. J. *J. Mater. Res.* **1992**, *7*, 784–787.
(45) Birkholz, M.; Fewster, P. F. *Thin Film Analysis by X-Ray Scattering*; Wiley−VCH Verlag GmbH & Co. KGaA: Weinheim, Germany, 2006; p 356.
(46) Karabacak, T.; Mallikarjunan, A.; Singh, J. P.; Ye, D.; Wang, G.-C.; Lu, T.-M. *Appl. Phys. Lett.* **2003**, *83*, 3096–3098.
(47) Huang, J. S.; Xu, Z.; Yang, Y. *Adv. Funct. Mater.* **2007**, *17*, 1966–1973.
(48) Hau, S. K.; Yip, H. L.; Ma, H.; Jen, A. K.-Y. *Appl. Phys. Lett.* **2008**, *93*, 233304.
(49) Hau, S. K.; Cheng, Y. J.; Yip, H. L.; Zhang, Y.; Ma, H.; Jen, A. K. Y. *ACS Appl. Mater. Interfaces* **2010**, *2*, 1892–1902.
(50) Lim, Y. F.; Lee, S.; Herman, D. J.; Lloyd, M. T.; Anthony, J. E.; Malliaras, G. G. *Appl. Phys. Lett.* **2008**, *93*, 193301.
(51) Ma, H.; Yip, H. L.; Huang, F.; Jen, A. K. Y. *Adv. Funct. Mater.* **2010**, *20*, 1371–1388.
(52) Hsieh, C. H.; Cheng, Y. J.; Li, P. J.; Chen, C. H.; Dubosc, M.; Liang, R. M.; Hsu, C. S. *J. Am. Chem. Soc.* **2010**, *132*, 4887–4893.
(53) Bao, Z. N.; Lovinger, A. J. *Chem. Mater.* **1999**, *11*, 2607–2612.
(54) Ewbank, P. C.; Loewe, R. S.; Zhai, L.; Reddinger, J.; Sauve, G.; McCullough, R. D. *Tetrahedron* **2004**, *60*, 11269–11275.
(55) Worfolk, B. J.; Rider, D. A.; Elias, A. L.; Thomas, M.; Harris, K. D.; Buriak, J. M. *Adv. Funct. Mater.* **2011**ASAP.
(56) Harris, K. D.; Westra, K. L.; Brett, M. J. *Electrochem. Solid-State Lett.* **2001**, *4*, C39–C42.
(57) Huang, J. S.; Xu, Z.; Yang, Y. *Adv. Funct. Mater.* **2007**, *17*, 1966 1973.
(58) Liao, H.; Chen, L.; Xu, Z.; Li, G.; Yang, Y. *Appl. Phys. Lett.* **2008**, *92*, 173303.
(59) Rider, D. A.; Harris, K. D.; Wang, D.; Bruce, J.; Fleischauer, M. D.; Tucker, R. T.; Brett, M. J.; Buriak, J. M. *ACS Appl. Mater. Interfaces* **2009**, *1*, 279–288.
(60) Motiei, L.; Yao, Y.; Choudhury, J.; Yan, H.; Marks, T. J.; van der Boom, M. E.; Facchetti, A. *J. Am. Chem. Soc.* **2010**, *132*, 12528–12530.
(61) Mihailetchi, V. D.; Xie, H.; de Boer, B.; Popescu, L. M.; Hummelen, J. C.; Blom, P. W. M.; Koster, L. J. A. *Appl. Phys. Lett.* **2006**, *89*, 012107.
(62) Perez, M. D.; Borek, C.; Forrest, S. R.; Thompson, M. E. *J. Am. Chem. Soc.* **2009**, *131*, 9281–9286.
(63) Ohno, T. R.; Chen, Y.; Harvey, S. E.; Kroll, G. H.; Weaver, J. H.; Haufler, R. E.; Smalley, R. E. *Phys. Rev. B* **1991**, *44*, 13747–13755.
(64) Li, G.; Chu, C.-W.; Shrotriya, V.; Huang, J.; Yang, Y. *Appl. Phys. Lett.* **2006**, *88*, 253503.
(65) Shirley, E. L.; Louie, S. G. *Phys. Rev. Lett.* **1993**, *71*, 133–136.
(66) Ren, S. L.; Wang, Y.; Rao, A. M.; McRae, E.; Holden, J. M.; Hager, T.; Wang, K. A.; Lee, W. T.; Ni, H. F.; Selegue, J.; Eklund, P. C. *Appl. Phys. Lett.* **1991**, *59*, 2678–2680.
(67) Duclos, S. J.; Haddon, R. C.; Glarum, S. H.; Hebard, A. F.; Lyons, K. B. *Solid State Commun.* **1991**, *80*, 481–484.